Judd-Ofelt analysis and laser investigations of Nd^{3+}-doped $Gd_{1-x}Sc_xCa_4O(BO_3)_3$ single crystal

L. GHEORGHE*, C. GHEORGHE
National Institute R&D for Laser, Plasma and Radiation Physics, Laboratory of Solid-State Quantum Electronics, P.O. Box MG 36, 077125, Bucharest-Magurele, Romania

Nonlinear optical (NLO) crystal of $Gd_{0.92}Sc_{0.02}Nd_{0.06}Ca_4O(BO_3)_3$ (Nd: GdScCOB) crystal has been grown by the Czochralski method. The high resolution and polarized spectroscopic data of Nd^{3+} in GdScCOB crystal were carried out and analyzed in the framework of the Judd - Ofelt theory. The polarized emission cross-sections for the $^4F_{3/2} \rightarrow {}^4I_{9/2}$ and $^4F_{3/2} \rightarrow {}^4I_{11/2}$ Nd^{3+} transitions of special interest for laser application were determined. Near-infrared laser emission at 1061 nm was achieved under cw Ti: sapphire end pumping at 812 nm. For propagation along the Z-axis, laser emission polarized parallel to the Y-axis was obtained. This result offers the opportunity to achieve type I SFD of Nd^{3+} emission in the ZX plane which presents a non-linearity approximately three times larger than XY plane.

(Received February 278, 2012; April 11, 2012)

Keywords: Self-frequency doubling, Czochralski method, Judd-Ofelt analysis, Laser emission

1. Introduction

All-solid-state laser sources are of special importance because of the advantages of this technology including compactness of the devices, efficiency, low maintenance and low cost. Moreover, many of the used crystals can be pumped by commercially available laser diodes, for example around 800 or 980 nm. Self-frequency converting crystals can generate wavelengths from the UV up to the infrared range which can be used for a variety of applications such as color displays, high density optical data storage, laser printing, biotechnology, medicine, submarine communications, gas-laser replacement, eye-safe generation, transparent atmosphere applications, etc.

Specific wavelengths can be achieved by direct laser operation of the most well-known luminescent ions: Nd^{3+} (1.06, 1.3 μm), Yb^{3+} (1.03 μm), Er^{3+} (1.5 μm), Ho^{3+} (2 μm), Tm^{3+} (2 μm), Cr^{3+} (0.7–1 μm) (this is a non-exhaustive list) incorporated in a suitable crystal. New wavelengths can be reached from frequency conversion of a given laser emission with the help of a nonlinear optical process. The process can originate from the second or third order nonlinear polarization in non-centrosymmetric crystals. The nonlinear crystal can be located outside the laser cavity or inside (intra-cavity frequency conversion). The latter device is widely used to obtain the visible range of wavelengths. Attractive crystals for frequency conversion are bi-functional laser and nonlinear optical (NLO) materials in which the laser effect and the nonlinear optical phenomena occur simultaneously inside the same host, simplifying the device.

In the last five decades, many NLO crystals were discovered. However, not all of them are good enough for practical applications. Some of the more important NLO crystals that are used in current commercial applications include $KTiOPO_4$ (KTP) [1], KH_2PO_4 (KDP), β-BaB_2O_4 (BBO) [2], LiB_3O_5 (LBO) [3] and periodically poled $LiNbO_3$ (PPLN) [4], etc. All of them are used for frequency conversion with a compatible laser system. Despite of the wider usage, essentially all of these crystals melt incongruently with the exception of $LiNbO_3$, so they all have to be grown by flux method, which makes them expensive, limited in size. Sometimes, even the crystal purity is questionable. The requirements to be an excellent NLO crystal include high nonlinear coefficients, large birefringence for phase matching, high transparency for the wavelengths of interest, non-hygroscopicity, high optical damage threshold, high thermal conductivity, and good thermal mechanical properties with high fracture toughness. Finally, the feasibility to produce large crystals at low cost is also highly desirable. NLO crystals allow fixed wavelength coherent light sources to be converted to the wavelength of application by several nonlinear conversion schemes, including second/third harmonic generation (SHG/THG), sum/difference frequency mixing, optical parametric oscillation or amplification. This has prompted us to search for new NLO materials exhibiting congruent melting which could be grown from the melt using the Czochralski pulling method. This technique is used to grow industrial crystals, such as the Nd-doped YAG laser material.

NLO crystals are not only useful for frequency conversion but also as self-frequency doubling (SFD) active laser sources. Since the first demonstration of SFD laser action in the green region from Nd-doped MgO:$LiNbO_3$ [5], a great effort was focused on searching new nonlinear laser crystals capable of generating SFD laser radiation in the visible. Up to now, extensive researches have been developed in Nd^{3+}-doped $YAl_3(BO_3)_4$ [6 - 9], $GdAl_3(BO_3)_4$ [10 - 12], $YCa_4O(BO_3)_3$

and $GdCa_4O(BO_3)_3$ [13 – 18], $BiBa_3O_6$ [19], $Ba_5NaNb_5O_{15}$ [20, 21], $Cd_3Y(BO_3)_3$ [22], ZnO:$LiNbO_3$ [23], $Ce_{1-x}Gd_xSc_3(BO_3)_4$ [24], $La_2CaB_{10}O_{19}$ [25], etc. Among these crystals, the best performances were obtained by using Nd: $YAl_3(BO_3)_4$ (NYAB) and Nd: $GdAl_3(BO_3)_4$ (NGAB) SFD crystals [26-28]. However, these two non-congruent melting crystals suffer from growing difficulties. By comparison, the SFD crystal Nd: $GdCa_4O(BO_3)_3$ (Nd: GdCOB) is much easier to grow and samples of 5 cm in diameter and 12 cm in length have already been obtained [15]. More than that, by doping of GdCOB with rare earth (RE) ions it is possible to achieve a significant increase of the photoinduced second-order susceptibility (even without the external photoinducing beam), and also to extend the applicability of RE-doped GdCOB crystals in different optoelectronic devices. In the case of doping with Pr^{3+} ions the SHG shows and increase of at least 35% under influence of photoinducing nitrogen laser (λ = 377 nm) power [29].

Recently, we have developed a substitutional solid solution of $Gd_{1-x}Sc_xCa_4O(BO_3)_3$ - GdScCOB crystal with controllable birefringence. Large and good optical quality crystals of GdScCOB have been grown by Czochralski technique, and oriented crystal samples up to several centimeters in length were relatively easily obtained [30, 31]. They are efficient biaxial NLO crystals (the effective nonlinear coefficients were found to be in the range of 0.5 to 0.6 pm/V at about 800 nm) [32] with large transparency range (from 320 to 2700 nm), high damage threshold (up to 1 GW/cm^2 at 1064 nm, 6 ns pulses), and non-hygroscopicity. Doped with Nd^{3+} they can be used as SFD crystals, which combine laser and nonlinear properties for intracavity transformation of the fundamental infrared laser wavelength into blue, green, or red emission. Diode pumping is also favored by the fairly good absorption of Nd^{3+} ions in the region of high power near-infrared laser diodes.

This paper reports the growth and spectroscopic characteristics of $Gd_{0.92}Sc_{0.02}Nd_{0.06}Ca_4O(BO_3)_3$ crystal. The emission cross-sections for $^4F_{3/2} \rightarrow {}^4I_{9/2}$ and $^4F_{3/2} \rightarrow {}^4I_{11/2}$ Nd^{3+} transitions of special interest for laser application were determined. Laser performances at 1.06 μm have been also investigated.

2. Experimental

A single crystal of $Gd_{1-x-y}Sc_xNd_yCa_4O(BO_3)_3$, with x = 0.2 and y = 0.07 in the synthesized material, was grown by using the conventional Czochralski method with iridium crucible and rf heating. The crystal was grown under a nitrogen atmosphere, and the diameter of the crystal was controlled by a computer through the feedback of weight measurement. The pulling rate was 0.8 - 1.0 mm/h, and the rotation rate was 30 – 35 rpm. A <010> - oriented single crystal of pure $GdCa_4O(BO_3)_3$ (GdCOB) was used as seed. As much as 20% of the melt was converted into a single crystal in approximately one week. The growth temperature was about 1480 ± 10º C. The grown crystal is highly transparent, nonhygroscopic, and chemically stable. Fig. 1 shows the as-grown $Gd_{1-x-y}Sc_xNd_yCa_4O(BO_3)_3$ crystal with dimensions of about 20 mm in diameter and 110 mm in length. The grown crystal has good mechanical properties, which make it easier for cutting and polishing. Chemical composition of the grown crystal was determined by means of inductively coupled plasma (ICP) and the crystal composition was found to be $Gd_{0.92}Sc_{0.02}Nd_{0.06}Ca_4O(BO_3)_3$ (Nd: GdScCOB).

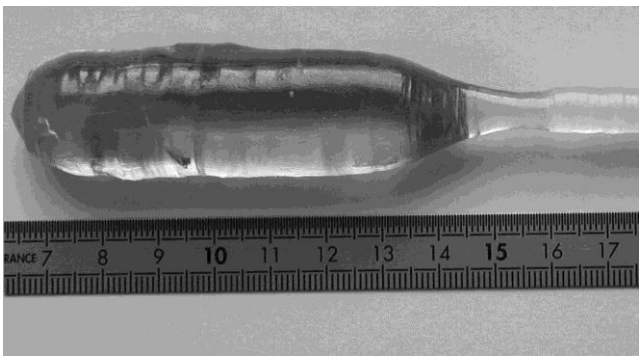

Fig. 1. Photograph of the as-grown $Gd_{0.92}Sc_{0.02}Nd_{0.06}Ca_4O(BO_3)_3$ single crystal.

The compositional uniformity of the grown crystal along the growth direction has been also examined by microprobe analyses on the samples exerted from the beginning, middle, and end of the crystal, and a compositional uniformity better than 0.5 at. % was obtained. This is due to the optimization of the crystal growth conditions and thermal gradients during crystal growth, as well as the relatively small fraction of crystallization from the melt (20%). The refractive indices of grown crystal (n_x, n_y and n_z) were measured by the minimum deviation technique. Several monochromatic sources were used to measure the values of refractive indices as function of wavelength.

High-resolution (0.3 cm^{-1}) spectral measurements at room temperature and 10 K of Nd (6 at. %) in GdScCOB crystal were carried out. Polarized room temperature absorption spectra were recorded in the range from 400 to 2000 nm using a setup consisting of a Jarell Ash monochromator, S20 and S1 photomultipliers, Si and Ge photodiodes and a Lock-in amplifier on line with a computer. For low temperature spectra, the samples were cooled down to 10 K in a closed cycle He refrigerator ARS-2HW. Polarized room temperature emission spectra were obtained under excitation from a continuous-wave (cw) Ti: sapphire laser – Solar II pumped with a Nd: YAG laser. Laser investigations of $Gd_{0.92}Sc_{0.02}Nd_{0.06}Ca_4O(BO_3)_3$ crystal were carried out using a plane-concave laser resonator end pumped with a cw Ti: sapphire laser.

3. Results and discussion

3. 1. Absorption properties and Judd-Ofelt analysis

Rare earth calcium oxyborate family $ReCa_4O(BO_3)_3$ (Re = Gd, Y, La) are among recent NLO crystals that have a very promising future. This family was first studied with the now well-known $GdCa_4O(BO_3)_3$ compound named GdCOB [33]. $ReCa_4O(BO_3)_3$ crystal family offers a unique opportunity to study the structure - properties relations because of its wide variety of compositions. It is possible in this oxyborate family for example to tune the composition in order to get good NLO properties for particular wavelength frequency conversion, as we already demonstrated in the case of $Gd_{1-x}Sc_xCa_4O(BO_3)_3$ crystals [31, 32]. Similar to GdCOB, Nd: GdScCOB grown crystal is monoclinic with a single position of Cs symmetry for Gd^{3+} ions, while Ca^{2+} ions occupy two sites of C_1 symmetry, $Ca^{2+}(1)$ and Ca^{2+} (2). According to the ionic radii [34], Sc^{3+} and Nd^{3+} ions could enter in any of the three cationic sites. The preference of Nd^{3+} for Gd^{3+} sites and the nature of additional three minority Nd^{3+} centers were outlined previously [35]. Two of them were associated with Nd^{3+} in Gd^{3+} sites slightly perturbed by charged intrinsic lattice defects of nonstoichiometric or inversion $Gd^{3+} \leftrightarrow Ca^{2+}$ type, while the third Nd^{3+} center is assigned to Nd^{3+} in a Ca^{2+} site. An appropriate transition for the study of different environments of Nd^{3+} is $^4I_{9/2} \rightarrow {}^2P_{1/2}$. At very low temperatures, only the lowest sublevel of $^4I_{9/2}$ ground state is populated, so the absorption spectrum corresponding to this transition presents only one peak for each type of Nd^{3+} environment. The absorption spectra (at 10 K) corresponding to the $^4I_{9/2} \rightarrow {}^2P_{1/2}$ transition in Nd: GdScCOB and in the reference crystal of Nd: GdCOB with the same Nd concentration (6 at. %), are presented in Fig. 2. As we can observe, the obtained spectra are similar, consisting of an intense peak (at 432 nm), which corresponds to neodymium in the gadolinium site and three other peaks of much lower intensities, located at - 0.8, - 0.35 and + 0.55 nm from the majority peak, marked with a "*" sign in Fig. 2. No other supplementary peaks were observed for Nd: GdScCOB crystal. The Nd^{3+} lines in both crystals are almost Gaussian, but they are wider in GdScCOB indicating an inhomogeneous broadening of the absorption peaks which implies a higher disorder around Nd^{3+} ions in this crystal. This is explained by the insertion of small Sc^{3+} ions in Nd: GdCOB structure which leads to an increase of the statistical disorder of the occupancy of the cationic sites.

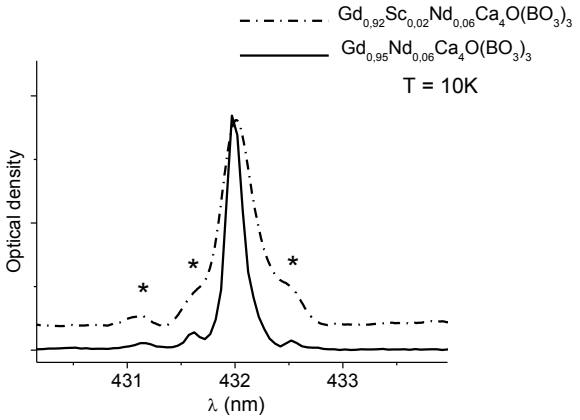

Fig. 2. Satellite structure of $^4I_{9/2} \rightarrow {}^2P_{1/2}$ Nd^{3+} (6 at. %) transition in GdCOB and GdScCOB at 10K.

In general, the inhomogeneous broadening is determined by point lattice defects, stresses induced by dimensional misfit, ion-ion interaction, etc. As shown previously [36, 37], the point defects that determine only local strains led to a Lorentz line shape at low concentration and Gaussian at large concentration. An almost Gaussian line shape is induced by charged defects [36]. The main intrinsic defects in GdCOB and GdScCOB are charged defects related to the nonstoichiometric or inversion $Gd^{3+} \leftrightarrow Ca^{2+}$ type, and additionally $Sc^{3+} \leftrightarrow Ca^{2+}$ type in the case of GdScCOB crystal. Taking into account that the ionic radius of Sc^{3+} ions is much smaller than that of Gd^{3+} ions (r_{Sc3+} = 0,75 Å and r_{Gd3+} = 0,94 Å in coordination 6 [34]), the occupancy disorder of Gd and Ca(1) sites increase with the increasing of Sc content. According to Ilyukhin et al. [38], the disorder in $Gd_{1-x}Sc_xCa_4O(BO_3)_3$ type crystals is much larger than in $GdCa_4O(BO_3)_3$ (14% Ca^{2+} in the sites of Gd^{3+}) Therefore, we can assume that the insertion of small Sc^{3+} ions in Nd: GdCOB structure contribute to the inhomogeneous broadening of Nd^{3+} absorption lines as consequence of the large Sc^{3+} - Gd^{3+} and Sc^{3+} - Ca^{2+} dimensional misfits, and also of the difference between electric charges of Sc^{3+} and Ca^{2+} ions.

A cubic Nd: GdScCOB crystal sample was cut and polished with each face oriented perpendicular to one crystallophysic axes (X, Y, Z), and different room temperature spectra were recorded with polarization of incident light parallel to X, Y and Z, respectively. The absorption spectra show important polarization effect for different Nd^{3+} transitions. According to our interest to obtain self-frequency doubling lasers pumped around 800 nm, details of polarized absorption spectra around 532 nm and 800 nm are shown in Figs. 3 and 4, respectively.

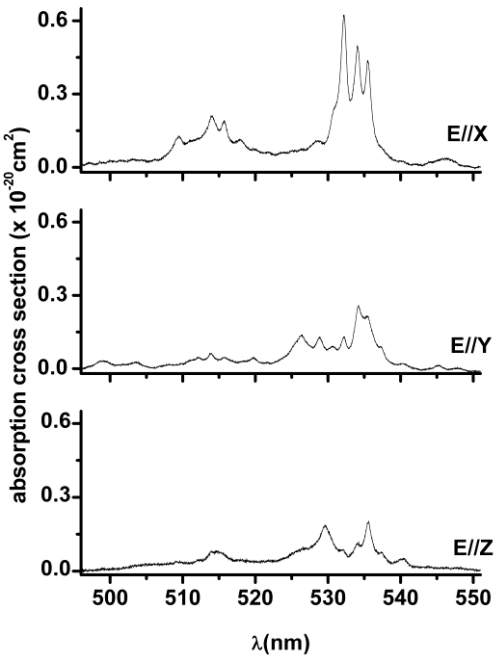

Fig. 3. Polarized absorption spectra of Nd: GdScCOB at 300 K in the range 490 – 550 nm.

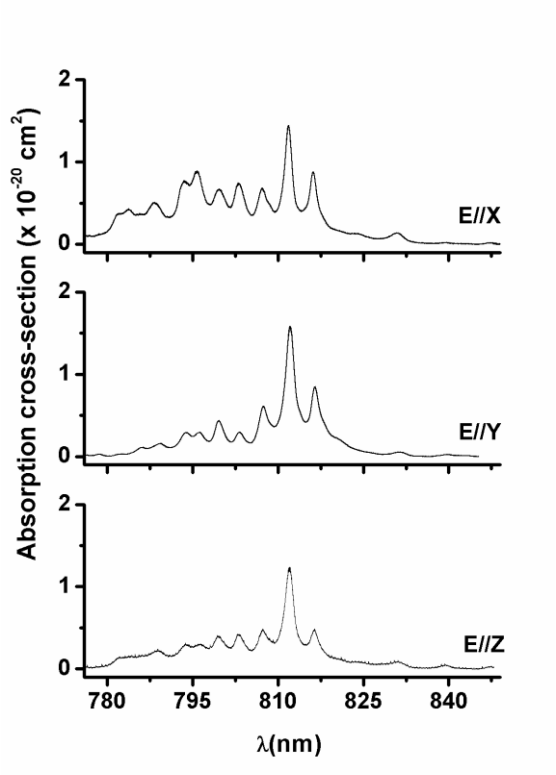

Fig. 4. Polarized absorption spectra of Nd: GdScCOB at 300 K in the range 770 - 850 nm.

The determined absorption cross sections are as follows: $\sigma_x = 1.43 \times 10^{-20}$ cm^2, $\sigma_y = 1.61 \times 10^{-20}$ cm^2 and $\sigma_z = 1.24 \times 10^{-20}$ cm^2 at 812 nm, and $\sigma_x = 0.53 \times 10^{-20}$ cm^2, $\sigma_y = 0.15 \times 10^{-20}$ cm^2 and $\sigma_z = 0.07 \times 10^{-20}$ cm^2 at 532 nm. It is important to note that at 812 nm Nd: GdScCOB crystal presents the highest absorption cross section for polarization parallel to the Y-axis, unlike the Nd: GdCOB where the polarization parallel to the X-axis gives the best absorption cross section [13]. The absorption cross sections at 532 nm are really weak, which is very favorable for SFD of the infrared laser emission at ~ 1.064 μm with a very low reabsorption at ~ 532 nm.

The calculations of the fundamental spectral parameters of Nd: GdScCOB based on the Judd-Ofelt (J-O) theory [39, 40] are important for the evaluation of the potential of a material for laser emission. The analysis of Nd: GdScCOB single crystal in the framework of the J-O theory has not been performed before. The procedure is briefly described by formulas given below for application. Eight room temperature absorption lines were used to determine the J-O parameters. The electric dipole line strength S (J→J') for different Nd^{3+} transitions starting from the $^4I_{9/2}$ fundamental level can be expressed as:

$$S_{calc}^{ed} = \sum_{t=2,4,6} \Omega_t \left| \left\langle 4f^n [S,L] J \left\| U^{(t)} \right\| 4f^n [S',L'] J' \right\rangle \right|^2 \quad (1)$$

where $\left\langle \left\| U^{(t)} \right\| \right\rangle$ are the reduced matrix elements corresponding to the transition from J to J' manifold of the $U^{(t)}$ irreducible tensor forms of the electric dipole operator [41], and the Ω_t are phenomenological J-O parameters. The magnetic dipole (md) transitions are allowed between states of the $4f^3$ configuration but in this case, the contribution of magnetic–dipole transitions to the line intensity and luminescence parameters was neglected because it is very small in comparison with that of the electric–dipole transitions.

The electric dipole line strength of a transition can also be determinate from the absorption measurements.

$$S_{meas}(J \to J') = \frac{3ch(2J+1)n}{N_0 3\pi^3 \overline{\lambda}} \left[\frac{9}{(n^2+2)^2} \right] \Gamma \quad (2)$$

where c is the speed of light, h is the Planck constant, N_0 is the Nd^{3+} ion concentration (2.74×10^{20} ions/cm^3), n is the crystal index of refraction, $\overline{\lambda}$ is the mean wavelength of the absorption band that corresponds to the J→J' transition, $\Gamma = \int k(\lambda) d(\lambda)$ is the integrated absorption coefficient, k(λ) is the wavelength dependent absorption coefficient. The refractive indices were obtained by a least-squares fit of the measured indices to one-pole Sellmeier dispersion equations [41]. The phenomenological J-O parameters Ω_t (t = 2, 4 and 6) were estimated from a least-squares fitting between the measured and calculated values of S (J→J'), treating Ω_t as adjustable parameters (Table 1). The mean wavelength, the refractive indices, the measured and calculated line strengths for several Nd^{3+} transitions in GdScCOB crystal,

and the rms (root mean square) deviation for each polarization are also given in Table 1. The average value of rms deviation is 0.262×10^{-20} cm^2. The link between polarized intensity parameters and conventional J-O intensity parameters is given by $\Omega = (\Omega_x+\Omega_y+\Omega_z)/3$.

The J-O parameters Ω_t for Nd: GdScCOB crystal and the corresponding values of these parameters for Nd: GdCOB [13, 42] and Nd: YCOB [43] crystals are presented in Table 2. As is seen, the Ω_2 parameter for Nd: GdScCOB is higher than the corresponding parameter for other Nd-doped crystals belonging to the $ReCa_4O(BO_3)_3$ family. At the same time, the intensity parameters Ω_4 and Ω_6 of Nd: GdScCOB crystal does not differ essentially from the corresponding parameters of other crystals. The explanation of the specific features of the changes in the intensity parameters Ω_t for Pr^{3+}, Nd^{3+}, Er^{3+}, and Tm^{3+} ions in Y_2O_3 crystals as compared to those for LaF_3 crystals doped with the corresponding ions was proposed by Krupke [44] with due regard for the assumption made by Judd [39], according to which the hypersensitivity of particular transitions or RE is associated with the specific features of the local environment and, correspondingly, with the type of point symmetry of RE ion in the crystal matrix. According to this assumption, the increasing of the Ω_2 parameter for Nd^{3+} ions in GdScCOB in comparison to other Nd-doped $ReCa_4O(BO_3)_3$ crystals, point to the presence in Nd: GdScCOB crystal of Nd optical centers with Cs and lower local environment symmetries determined by the insertion of Sc^{3+} ions in the GdCOB matrix, which induce a larger disorder around Nd^{3+} ions.

By using the J-O parameters a series of other spectroscopic parameters were estimated. The total spontaneous electric dipole emission transition probabilities from the excited state J to the terminating state J' are given by the expression:

$$A_{JJ'}^{ed} = \frac{64\pi^4 e^3}{3h(2J+1)\bar{\lambda}^3}\frac{n(n^2+2)^2}{9}\sum_{t=2,4,6}\Omega_t\left|\left\langle (S,L)J\right\|U^t\left\|(S',L')J'\right\rangle\right|^2 \quad (4)$$

The radiative lifetime τ_r for an excited state J and the fluorescence branching ratios $\beta(J\rightarrow J')$ for the various emission transitions from this state can be then calculated by: $\tau_r = \frac{1}{\sum A(J\rightarrow J')}$, and $\beta(J\rightarrow J') = \frac{A(J\rightarrow J')}{\sum_{J'} A(J\rightarrow J')}$.

The calculated values of the electric dipole spontaneous emission probabilities ($A_{JJ'}$), branching ratios ($\beta_{JJ'}$) and radiative lifetime for each polarization of the main emission transitions of Nd^{3+}: GdScCOB are presented in Table 3. The average estimated radiative lifetime for Nd^{3+} $^4F_{3/2}$ level is about 753 μs.

From the luminescence decay curve of the $^4F_{3/2}$ level of Nd (6 at. %) in GdScCOB crystal the fluorescence lifetime was determined to be 105 μs at room temperature. This value is comparable with the fluorescence lifetime obtained in the case of Nd: GdCOB crystal, 98 μs [13]. As is well known, in Nd-doped crystals the high energy phonons are usually considered to make the dominant contribution to the multiphonon relaxation from the $^4F_{3/2}$ state to next lower state $^4I_{15/2}$ since they can interact with electrons to conserve energy in the lowest-order process. The large multiphonon non-radiative relaxation rate will lead to the low quantum efficiency. In general, the largest phonon frequency associated with the main oscillation bands of the planar group $(BO_3)^{3-}$ centered at 1250 cm^{-1} make the borate crystals to have low fluorescence quantum efficiency [13].

3.2. Stimulated emission cross-section

Polarized room temperature emission spectra corresponding to Nd^{3+} $^4F_{3/2}(1) \rightarrow {}^4I_J$ transitions, under selective excitation were obtained by pumping in 812 nm region. From the emission spectra, the stimulated emission cross section between $^4F_{3/2}$ and ^4I_J manifolds at wavelength λ for anisotropic medium of refractive index n is calculated according to the Füchtbauer–Ladenburg method:

$$\sigma(\lambda) = \frac{\lambda^5 A(J\rightarrow J')}{8\pi n^2 c}\frac{I(\lambda)}{\int \lambda I(\lambda)d\lambda} \quad (5)$$

where I(λ) is the fluorescence intensity at wavelength λ, A (J→J') the spontaneous emission probability from the initial manifold $^4F_{3/2}$ to the terminal manifold ^4I_J (J'= 9/2 and 11/2,), c speed of light, n the refraction index. The obtained emission cross sections peaks corresponding to the $^4F_{3/2} \rightarrow {}^4I_{9/2}$ and $^4F_{3/2} \rightarrow {}^4I_{11/2}$ transitions of Nd^{3+} in GdScCOB crystal are shown in Figs. 5 and 6, respectively.

Table 4 summarizes the important absorption peak cross sections. For these transitions, the highest emission cross sections are those with polarization parallel to the Y-axis, contrary to Nd: GdCOB crystal where the polarization parallel to the X-axis gives the highest emission cross sections [13].

Table 1. Measured and calculated absorption line strength of Nd^{3+} in GdScCOB single crystal at 300K1.

Transition from $^4I_{9/2}$	E//X				E//Y				E//Z			
	$\bar{\lambda}$ (nm)	n	S_{meas} ($10^{-20}cm^2$)	S_{calc} ($10^{-20}cm^2$)	$\bar{\lambda}$ (nm)	n	S_{meas} ($10^{-20}cm^2$)	S_{calc} ($10^{-20}cm^2$)	$\bar{\lambda}$ (nm)	n	S_{meas} ($10^{-20}cm^2$)	S_{calc} ($10^{-20}cm^2$)
$^4F_{3/2}$	879.35	1.684	0.326	0.370	881.36	1.710	0.225	0.254	880.32	1.719	0.675	0.595
$^4F_{5/2}$, $^2H_{9/2}$	808.15	1.686	1.642	1.299	807.46	1.712	1.922	1.586	805.40	1.722	1.996	1.613
$^4F_{7/2}$, $^4S_{3/2}$	745.31	1.688	1.120	1.320	745.98	1.714	1.667	1.862	743.64	1.724	1.266	1.492
$^4F_{9/2}$	684.23	1.690	0.140	0.094	681.51	1.717	0.073	0.122	681.21	1.727	0.298	0.113
$^2H_{11/2}$, $^4G_{5/2}$, $^2G_{7/2}$	590.56	1.696	3.417	3.397	591.41	1.723	3.145	3.124	590.49	1.732	3.699	3.654
$^2K_{13/2}$, $^4G_{7/2}$, $^4G_{9/2}$	533.71	1.701	0.382	0.661	534.99	1.727	0.252	0.635	533.66	1.737	0.322	0.893
$^2K_{15/2}$, $^2G_{9/2}$, $^2D_{3/2}$, $^4G_{11/2}$	469.92	1.708	0.130	0.120	466.95	1.736	0.155	0.131	470.38	1.744	0.155	0.177
$^2P_{1/2}$	433.54	1.714	0.025	0.043	433.12	1.742	0.027	0.018	434.78	1.752	0.099	0.081
	$\Omega_2 = 2.94 \times 10^{-20}cm^2$ $\Omega_4 = 2.03\times 10^{-20}cm^2$ $\Omega_6 = 1.26 \times 10^{-20}cm^2$ rms = $0.230\times 10^{-20}cm^2$				$\Omega_2 = 3.04 \times 10^{-20}cm^2$ $\Omega_4 = 2.97 \times 10^{-20}cm^2$ $\Omega_6 = 0.97 \times 10^{-20}cm^2$ rms = $0.245 \times 10^{-20}cm^2$				$\Omega_2 = 2.64 \times 10^{-20}cm^2$ $\Omega_4 = 2.28 \times 10^{-20}cm^2$ $\Omega_6 = 2.09 \times 10^{-20}cm^2$ rms = $0.311 \times 10^{-20}cm^2$			

Table 2. The Judd-Ofelt strength parameters for Nd^{3+}-doped GdScCOB single crystal compared with Nd: GdCOB single crystals.

Materials	Ω_2 (10^{-20} cm^2)	Ω_4 (10^{-20} cm^2)	Ω_6 (10^{-20} cm^2)	τ_{rad} ($^4F_{3/2}$) (μs)	τ_{meas} ($^4F_{3/2}$) (μs)	Ref.
Nd: GdCOB	1.07	2.64	1.52	659	98	13
Nd: GdCOB	1.15	2.75	1.5		98	42
Nd: YCOB	1.20	2.87	1.32	601		43
Nd: GdScCOB	2.87	2.42	1.44	753	105	This work

Table 3. The calculated values of the total spontaneous emission transition probabilities ($A_{JJ'}$), branching ratios ($\beta_{JJ'}$) and radiative lifetime for the main emission transitions of Nd^{3+} in GdScCOB.

Transition	E//X					E//Y					E//Z				
	$\bar{\lambda}$ (nm)	n	S ($10^{-20}cm^2$)	$A^{ed}_{JJ'}$ (s^{-1})	$\beta_{JJ'}$	$\bar{\lambda}$ (nm)	n	S ($10^{-20}cm^2$)	$A^{ed}_{JJ'}$ (s^{-1})	$\beta_{JJ'}$	$\bar{\lambda}$ (nm)	n	S ($10^{-20}cm^2$)	$A^{ed}_{JJ'}$ (s^{-1})	$\beta_{JJ'}$
$^4F_{3/2}\rightarrow{}^4I_{9/2}$	879.35	1.684	0.375	457.19	0.39	881.36	1.710	0.265	315.5	0.24	880.32	1.719	0.601	746.8	0.48
$^4I_{11/2}$	1080.2	1.680	0.957	565.27	0.48	1080.2	1.706	1.914	772.8	0.6	1080.2	1.715	1.159	758.4	0.49
$^4I_{13/2}$	1371.6	1.677	0.416	139.25	0.11	1371.6	1.701	0.595	191.4	0.14	1371.6	1.710	0.463	152.3	0.09
$^4I_{15/2}$	1911.6	1.672	0.062	7.14	0.006	1911.6	1.693	0.0775	8.3	0.006	1911.6	1.700	0.071	7.2	0.004
	τ_r = 753 μs , τ_{mas} = 105 μs														

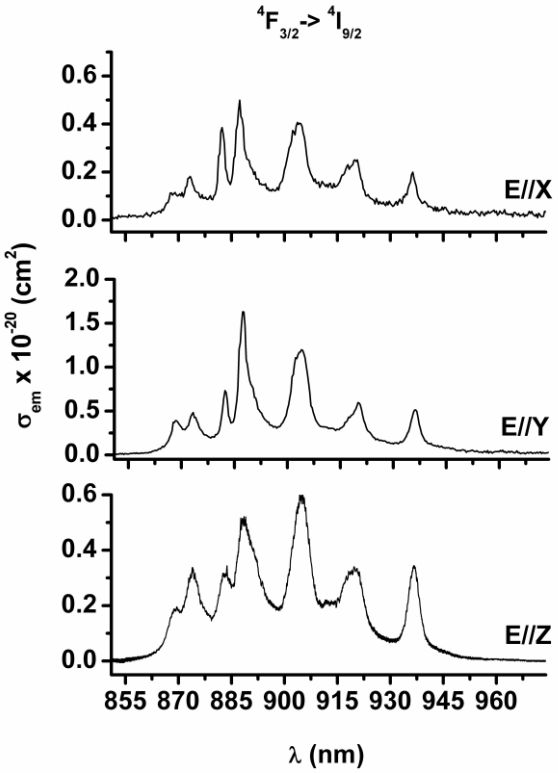

Fig. 5. Emission cross-section peaks corresponding to the $^4F_{3/2} \rightarrow {}^4I_{9/2}$ transitions of Nd^{3+} in GdScCOB crystal.

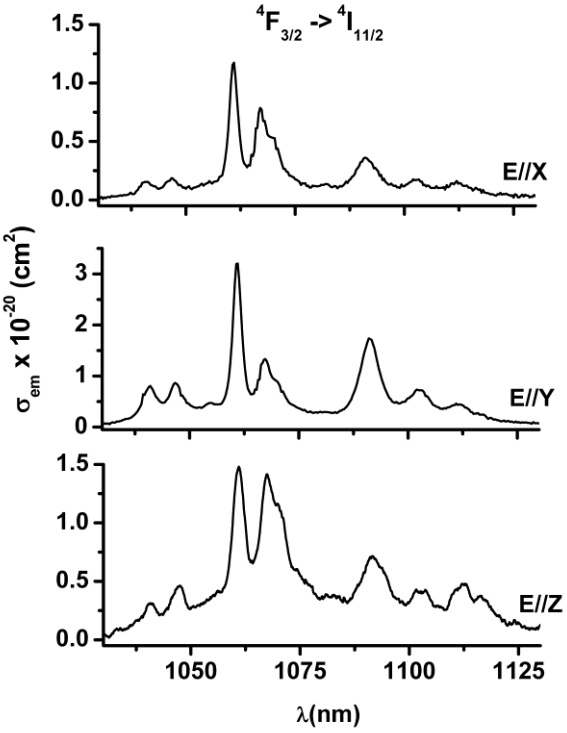

Fig. 6. Emission cross-section peaks corresponding to the $^4F_{3/2} \rightarrow {}^4I_{11/2}$ transitions of Nd^{3+} in GdScCOB crystal.

Table 4. The polarized emission cross section for principal emission lines of Nd^{3+} - doped $Gd_{0.92}Sc_{0.02}Nd_{0.06}Ca_4O(BO_3)_3$ single crystal.

$Gd_{0.92}Sc_{0.02}Nd_{0.06}Ca_4O(BO_3)_3$				
	λ (nm)	$\sigma_x \times 10^{-20}(cm^2)$	$\sigma_y \times 10^{-20}(cm^2)$	$\sigma_z \times 10^{-20}(cm^2)$
$^4F_{3/2} \rightarrow {}^4I_{9/2}$	887.3	0.49	1.63	0.47
	904.3	0.40	1.18	0.60
	920	0.25	0.59	0.34
	936	0.19	0.51	0.35
$^4F_{3/2} \rightarrow {}^4I_{11/2}$	1061	1.17	3.20	1.47
	1067	0.78	1.33	1.40
	1091	0.36	1.73	0.69

Based on this result, we can expect to obtain laser emissions at 936 and 1061 nm polarized parallel to the Y-axis for propagation along the Z-axis of the Nd: GdScCOB crystal. For the laser emission at 1061nm, this result is very important because it will make it possible to achieve type I SFD of the fundamental laser emission at 1061nm (transition $^4F_{3/2} \rightarrow {}^4I_{11/2}$) in the ZX plane which has the highest non-linearity. We note that in the case of GdCOB the effective nonlinear coefficient ($d_{eff} = d_{12}\cos\theta - d_{32}\sin\theta$) in the ZX plane is higher than the effective nonlinear coefficient ($d_{eff} = d_{13}\sin\varphi$) in XY plane. This is explained by the very high value of d_{32} coefficient (1.67 pm/V) compared to d_{13} coefficient (0.59 pm/V) [45]. In order to confirm if the insertion of Sc^{3+} ions in the Nd: GdCOB matrix leads to obtain infrared laser emission polarized parallel to the Y-axis, laser tests were performed.

3. 3. Laser experiments

Infrared laser experiments were performed under cw Ti: sapphire pumping at 812 nm. A parallelepipedic $Gd_{0.92}Sc_{0.02}Nd_{0.06}Ca_4O(BO_3)_3$ crystal sample oriented along crystallophysic axes was used. The length of the sample along the Z-axis (the direction of propagation) was

7 mm and both end faces were AR coated at 1061 nm. The pump beam was focused in the crystal by a 100 mm focal-length lens. The laser cavity consists of a planar input mirror highly reflective (HR) at 1061 nm and highly transmittive (HT) at 812 nm, and a concave output mirror (radius of curvature of 100 mm) with a transmission of 2 % at 1061 nm. The cavity length was about 100 mm. Laser emission of the $^4F_{3/2} \rightarrow {}^4I_{11/2}$ Nd^{3+} transition in GdScCOB crystal was obtained at 1061 nm. We obtained up to 251 mW of laser power for a maximum incident power of 1.67 W, with a slope efficiency (defined as the ratio of the output power to the absorbed pump power) of 31.4 % and a power threshold of about 300 mW. For propagation along the Z-axis, the polarization of the laser emission was parallel to the Y-axis, as it was expected from emission studies.

This result is remarkable because it opens new perspectives for type I SFD of laser emission at 1061 nm of the Nd-doped oxyborate matrices derived from GdCOB, containing Sc^{3+} ions. In fact, a partial substitution of Gd^{3+} by small ions such as Sc^{3+}, offers the opportunity to achieve type I SFD of neodymium emission in the ZX plane which presents a non-linearity approximately three times larger than XY plane (configuration usually adopted for SFD in Nd: GdCOB). A priori, the conversion efficiency should be approximately nine times larger (the conversion efficiency increases with the square of the effective nonlinear coefficient) in these conditions.

4. Conclusions

A single crystal of $Gd_{0.92}Sc_{0.02}Nd_{0.06}Ca_4O(BO_3)_3$ with large size and good optical quality has been grown by the Czochralski method. The main spectroscopic properties of Nd^{3+}-doped GdScCOB crystal have been determined for the three X, Y, and Z polarizations, based on the J-O theory. The phenomenological J-O parameters were determined to be $\Omega_2 = 2.87\times10^{-20}$ cm^2, $\Omega_4 = 2.42\times10^{-20}$ cm^2, and $\Omega_6 = 1.44\times10^{-20}$ cm^2. The obtained values are in agreement with the values obtained for other Nd-doped crystals from the $ReCa_4O(BO_3)_3$ family, and indicate that Nd: GdScCOB crystal contains Nd centers with Cs and lower local environment symmetries. By means of the J-O parameters calculated from the absorption spectra, the radiative transition rates, fluorescence branching ratios, and radiative lifetime of Nd^{3+} in GdScCOB were also calculated and analyzed. Near-infrared emission at 1061 nm corresponding to the $^4F_{3/2} \rightarrow {}^4I_{11/2}$ laser transition of Nd-doped GdScCOB crystal was achieved under cw Ti: sapphire end pumping at 812 nm. For now, we limited our study to low pump powers (maximum incident power of 1.67 W). For propagation along the Z-axis, laser emission polarized parallel to the Y-axis was obtained for the first time. This result is very important because it allows reviewing all studies concerning the type I SFD of the fundamental laser emission at 1061nm of Nd-doped $Re_{1-x}Sc_xCa_4O(BO_3)_3$ (Re = Gd, Y, La) oxyborate crystals, but this time in the ZX plane which has a non-linearity approximately three times larger than XY plane. This work is now in progress in our laboratory.

Acknowledgments

This work was supported by the "Partnerships" Romanian Research Programme - Contract No. 12105/2008, and "Ideas" Romanian Research Programme - Contract No. 491/2009.

References

[1] Z. Y. Ou, S. F. Pereira, E. S. Polzik, H. J. Kimble, Opt. Lett. **17**, 640 (1992).
[2] L. K. Cheng, W. R. Bosenberg, C. L. Tang, Prog. Cryst. Growth and Charact. Mater. **20,** 9 (1990).
[3] T. Izawa, R. Uchimura, S. Mtsui, T. Arichi, T. Yakuoh, OSA Technical Digest of Conference on Lasers and Electro-Optics, **6**, 322 (1998).
[4] G. D. Miller, R. G. Batchko, W. M. Tulloch, D. R. Weise, M. M. Fjer, R. L. Byer, Opt. Lett. **22,** 1834 (1997).
[5] T. Y. Fan, A. Cordova-Plaza, M. J. F. Digonnet, R. L. Byer, H. J. Shaw, J. Opt. Soc. Am. B **3**, 140 (1986).
[6] Z. Luo, A. Jiang, Y. Huang, M. Qiu, Chin. Phys. Lett. **6**, 440 (1989).
[7] Z. D. Luo, Prog. Nat. Sci. **4**, 504 (1994).
[8] J. Bartschke, R. Knappe, K.-J. Boller, R. Wallenstein, IEEE J. Quant. Electr. **33**, 2295 (1997).
[9] D. Jaque, J. Capmany, J. Garcia Sole, Appl. Phys. Lett. **74**, 1788 (1999).
[10] C. Tu, M. Qiu, Y. Huang, X. Chen, A. Jiang, Z. Luo, J. Cryst. Growth **208**, 487 (2000).
[11] A. Brenier, C. Tu, M. Qiu, A. Jiang, B. Wu, J. Li, J. Opt. Soc. Am. B **18**, 1104 (2001).
[12] A. Brenier, C. Tu, J. Li, Z. Zhu, B. Wu, Opt. Commun. **200**, 355 (2001).
[13] F. Mougel, G. Aka, A. Kahn-Harari, H. Hubert, J. M. Benitez, D. Vivien, Opt. Mater. **8,** 161 (1997).
[14] Q. Ye, L. Shah, J. Eichenholz, D. Hammons, R. Peale, M. Richardson, A. Chin, B. H. T. Chai, Opt. Commun. **164,** 33 (1999).
[15] G. Aka, E. Reino, P. Loiseau, D. Vivien, B. Ferrand, L. Fulbert, D. Pelenc, G. Lucas-Leclin, P. Georges, Opt. Mater. **26**, 431 (2004).
[16] C. Q. Wang, Y. T. Chow, W. A. Gambling, S. J. Zhang, Z. X. Cheng, Z. S. Shao, H. C. Chen, Opt. Commun. **174**, 471 (2000).
[17] A. Brenier, J. Nonlinear Opt. Phys. Mater. **12**, 349 (2003).
[18] S. Zhang, Z. Cheng, J. Han, G. Zhou, Z. Shao, C. Wang, Y. T. Chow, H. Chen, J. Cryst. Growth **206**, 197 (1999).
[19] A. Brenier, I. V. Kityk, A. Majchrowski, Opt. Commun. **203**, 125 (2001).
[20] G. Foulon, A. Brenier, M. Ferriol, M. T. Cohen-Adad, G. Boulon, J. Lumin **72-74**, 794 (1997).
[21] G. Foulon, M. Ferriol, A. Brenier, M. T. Cohen-Adad, M. Boudeulle, G. Boulon, Opt. Mat. **8**, 65 (1997).
[22] Z. Zhu, C. Tu, J. Li, B. Wu, J. Cryst. Growth **263,** 291 (2004).
[23] J. Capmany, D. Jaque, J. A. Sanz García, J. García Solé, Opt. Commun. **161**, 253 (1999).

[24] V. Ostroumov, K. Petermann, G. Huber, A. A. Ageev, S. Kutovoj, O. Kuzmin, V. Panyutin, E. Pfeifer, A. Hinz, J. Lumin. **72-74**, 826 (1997).
[25] Y. Wu, J. Zhang, G. Zhang, P. Fu, Y. Wu, J. Cryst. Growth **318,** 632 (2011).
[26] A. Brenier, Opt. Commun. **129,** 57 (1996).
[27] A. Brenier, J. Lumin. **91**, 121 (2000).
[28] D. Jaque, J. Capmany, J. A. Sanz García, A. Brenier, G. Boulon, J. García Solé, Opt. Mat. **13,** 147 (1999).
[29] T. Łukasiewicz, I. V. Kityk, M. Makowska-Janusik, A. Majchrowski, Z. Gałązka, H. Kaddouri, Z. Mierczyk, J. Cryst. Growth **237-239,** 641 (2002).
[30] L. Gheorghe, P. Loiseau, G. Aka, V. Lupei, J. Cryst. Growth **294**, 442 (2006).
[31] L. Gheorghe, P. Loiseau, G. Aka, Opt. Mater. **32**, 1283 (2010).
[32] M. T. Andersen, J. L. Mortensen, S. Germershausen, P. Tidemand-Lichtenberg, P. Buchhave, L. Gheorghe, V. Lupei, P. Loiseau, G. Aka, Opt. Express **15**, 4893 (2007).
[33] G. Aka, A. Kahn-Harari, D. Vivien, J. M. Benitez, F. Salin, J. Godard, Eur. J. Solid State Inorg. Chem **33**, 727 (1996).
[34] R. D. Shannon, Acta Crystallogr., Sect. A: Cryst. Phys. Diffr., Theor. Gen. Crystallogr. **32**, 751 (1976).
[35] A. Lupei; E. Antic-Fidancev, G. Aka, D. Vivien, P. Aschehoug, Ph. Goldner, F. Pelle, L. Gheorghe, Phys Rev B, **65**, 224518 (2002).
[36] A. M. Stoneham, Rev. Mod. Phys. **41,** 82 (1969).
[37] D. L. Orth, R. J. Mashl, J. L. Skinner, J. Phys.: Condens. Matter **5**, 2533 (1993).
[38] A. B. Ilyukhin, B. F. Dzhurinskii, Russ. J. Inorg. Chem. **38**, 917 (1993).
[39] B. R. Judd, Phys. Rev. **127**, 750 (1962).
[40] G. S. Ofelt, J. Chem.Phys. **37**, 511 (1962).
[41] W. Carnall, P. Field, B. Wybourne, J. Chem Phys. **42**, 3797 (1968).
[42] C. Maunier, J. L. Doualan, G. Aka, J. Landais, E. Antic-Fidancev, R. Moncorge, D. Vivien, Opt. Commun **184**, 209 (2000).
[43] H. R. Xia, W. Q. Zheng, S. J. Zhang, Z. X. Cheng, X. F. Cheng, Z. H. Yang, J. Appl. Phys. **92**, 5060 (2002).
[44] W. F. Krupke, Opt. Commun. **12**, 210 (1974).
[45] M. V. Pack, D. J. Darrell, A. V. Smith, G. Aka, B. Ferrand, D. Pelenc, JOSA B, **22**, 417 (2005).

*Corresponding author: lucian.gheorghe@inflpr.ro